

## Diffraction mathematical model of a laser speckle interferometer of transverse displacements of a scattering object

© L.A. Maksimova,<sup>1</sup> N.Yu. Mysina,<sup>1</sup> B.A. Patrushev,<sup>1,2</sup> V.P. Ryabukho<sup>1,2</sup>

<sup>1</sup> Institute of Precision Mechanics and Control Separate structural subdivision of the Federal State Budgetary Institution of Science of the Federal Research Center „Saratov Scientific Center of the Russian Academy of Sciences“, Saratov, Russia

<sup>2</sup> Saratov National Research State University n/a N.G. Chernyshevsky, Saratov, Russia  
E-mail: MaksimovaLA@yandex.ru

Received January 16, 2023

Revised January 16, 2023

Accepted January 16, 2023

On the basis of diffraction transformations of wave fields, a mathematical model of a speckle interferometer of transverse displacements of a scattering object has been developed and numerical modeling of speckle-modulated interference patterns and signals at the output of the interferometer has been performed. Numerical calculations of the spatial distribution of complex amplitudes of wave fields in an interferometer were used for modeling when the displaced scattering surface was illuminated by two obliquely incident laser Gaussian beams. A statistical numerical experiment was performed to determine the measurement error of the scattering surface displacement caused by the change of realizations of interfering speckle fields. The simulation results are in good agreement with the results of experimental studies of transverse displacements in the range up to 600 micrometers.

**Keywords:** interferometry, diffraction, interference, laser interferometer, speckle interferometry, interference pattern, speckle modulation, computer simulation.

DOI: 10.21883/TP.2023.04.55941.3-23

### Introduction

Interference patterns and signals generated at the output of laser speckle interferometers have a stochastic speckle-modulated character because almost all technical and biological objects studies by means of such an interferometer have a scattering surface. When reflected from such a surface, the scattered laser wave field acquires speckle modulation [1–3], which occurs because of the superposition and interference of waves scattered by microscopic inhomogeneities of the probed rough surface.

Methods of measurement and control based on the interference of light scattered by inhomogeneous surfaces allow investigating microdisplacements and microdeformations of technical and biological scattering objects [1–14] and assessing the roughness degree of the scattering surface [12,15]. In a number of practical problems of science, technology, and biomedical research, there is a practical need to measure the motion parameters of scattering objects, i.e., microdisplacements, velocity, and acceleration. A number of such problems are solved using speckle interferometers, in which the controlled scattering surface is illuminated by two laser beams incident at different angles [16–19].

Mathematical modeling is a necessary tool for studying the processes occurring in various measuring optical systems [20–23]. The development of a mathematical model of a speckle interferometer makes it possible to establish the limits of applicability of the method and estimate the

measurement errors. It also allows optimizing the speckle interferometer optical parameters [24,25]. The diffraction processes that take place in speckle interferometers are the basis for modeling complex measured signals in such interference systems and obtaining accurate results for system-level studies [12,26].

The purpose of this work was to develop a mathematical model of the speckle-modulated interference pattern and signal formation at the output of a speckle interferometer upon transverse displacements of the scattering object. The model makes it possible to reveal the properties and quantitative parameters of interference measuring signals, to analyze the reliability of experimental results and the accuracy of measurements, to make a correct assessment of possible measurement errors, and to identify their origin. To test the proposed mathematical model, we simulated the signals of the speckle interferometer by calculating numerically the spatial distribution of the complex amplitudes of diffractive wave fields, when the displaced scattering surface is illuminated by obliquely incident Gaussian laser beams, which are often used in practice. The development of the diffraction theory of interferometer signal formation is aimed at establishing the physical causes of the occurrence of the interferometer measuring signal upon a transverse displacement of the scattering surface, associated with the phase modulation of scattered wave fields, which does not require the use of Doppler effect ideas [27–32].

### 1. Diffraction interference patterns at the output of speckle interferometer of transverse displacement of the scattering object surface illuminated by Gaussian laser beams

To study the formation of the speckle-interferometer measuring signal, numerical simulation of interference speckle-modulated patterns at the output of the interferometer was performed. In the considered speckle interferometer of transverse displacements, the illuminating Gaussian laser beams are incident symmetrically on the scattering surface in the  $y, z$  plane at angles  $\theta$  and  $-\theta$  (Fig. 1). The optical axes of the beams do not cross at the surface, so that the centers of the illuminated spots are separated by  $2\Delta y$  in the incidence plane of the beams.

Figure 2 presents samples of simulated speckle-modulated interference patterns formed at the interferometer output and images of laser beam illuminated areas on the scattering surface. The interference fringes in the speckles are caused by the displacement of illuminated areas on the scattering surface and their period is determined by the equation  $\Lambda \approx \lambda z_s / 2\Delta y \approx \lambda / \alpha$ , where  $z_s$  is the distance from the scattering surface to the output plane of the interferometer  $\xi, \eta$  (Fig. 1),  $\alpha$  is the angle of convergence of interfering diffraction waves to the plane  $\xi, \eta$ . The transverse speckle size is  $\varepsilon_{\perp} \approx \lambda z_s / d$ , where  $d$  is the size of the illuminated area on the scattering surface. The fringes become invisible (Fig. 2, c), if the speckle size is smaller than the period of fringes,  $\varepsilon_{\perp} \leq \Lambda$ , which is equivalent to  $d \geq 2\Delta y$ .

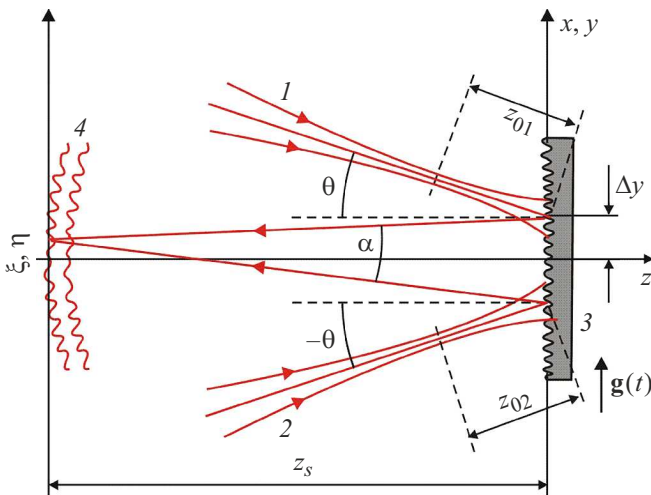


**Figure 1.** Scheme of illumination of a scattering surface by two Gaussian laser beams and formation of a diffraction speckle-modulated interference pattern at the output of the speckle interferometer of surface transverse displacements: 1, 2 — illuminating laser beams, 3 — object with a scattering surface,  $g(t)$  — vector of the surface transverse displacement, 4 — scattered diffraction wave fields at the output of the interferometer.

For the Gaussian beam incident at an angle  $\theta$ , in order to write the Gaussian beam complex amplitude distribution in the plane of incidence, it is necessary to perform a coordinate transformation, expressing coordinates  $x_0, y_0, z_0$ , in which the beam incidence angle is  $\theta = 0$ , in terms of new coordinates  $x, y, z$ , in which  $\theta \neq 0$ :

$$\begin{aligned} y_0 &= y \cos \theta + z \sin \theta, \\ z_0 &= z \cos \theta - y \sin \theta, \\ x_0 &= x. \end{aligned} \tag{1}$$

According to Eq. (1), the complex amplitude distribution for a Gaussian beam incident at an angle  $\theta$  on a scattering surface can be written in the following form [33]:

$$\begin{aligned} U(x, y, z) &= A \frac{w_0}{w(y, z)} \exp \left[ -\frac{(x^2 + (y \cos \theta + z \sin \theta)^2)}{w^2(y, z)} \right] \\ &\times \exp \left( i \frac{\pi}{\lambda R(y, z)} (x^2 + (y \cos \theta + z \sin \theta)^2) \right) \\ &\times \exp \left( i \arctg \left( \frac{\lambda(z \cos \theta - y \sin \theta)}{\pi w_0^2} \right) \right) \\ &\times \exp \left( i \frac{2\pi}{\lambda} (z \cos \theta - y \sin \theta) \right), \end{aligned} \tag{2}$$

where

$$w(y, z) = w_0 \left( 1 + \left( \frac{\lambda(z \cos \theta - y \sin \theta)}{\pi w_0^2} \right)^2 \right)^{0.5},$$

$$R(y, z) = (z \cos \theta - y \sin \theta) \left( 1 + \left( \frac{\pi w_0^2}{\lambda(z \cos \theta - y \sin \theta)} \right)^2 \right),$$

where  $\lambda$  is the laser beam wavelength,  $A$  is the real-valued amplitude assumed to be  $A = 1$  for convenience,  $w(y, z)$  is the amplitude beam radius,  $w_0$  is the beam waist radius,  $R(y, z)$  is the wave front curvature radius.

To study the phase distribution in the wave field formed in the interferometer, we determine the surface of equal phase in the incident Gaussian beam  $\varphi_1(x, y, z) = n\pi$  from Eq. (2) at the incidence angle  $\theta = 0$  for the initial phase  $\varphi_0 = 0$

$$\varphi_1(x, y, z) = n\pi = \frac{\pi}{\lambda R_1(z)} (x^2 + y^2) + \arctg \left( \frac{\lambda z}{\pi w_0^2} \right) + \frac{2\pi}{\lambda} z, \tag{3}$$

where

$$R_1(z) = z \left( 1 + \left( \frac{\pi w_0^2}{\lambda z} \right)^2 \right),$$

$n$  being the number of maximum or minimum.

From Eq. (3) we derive the equation of the equal phase surface  $\varphi_2(x, y, z) = n\pi$  for the nonzero incidence angle of

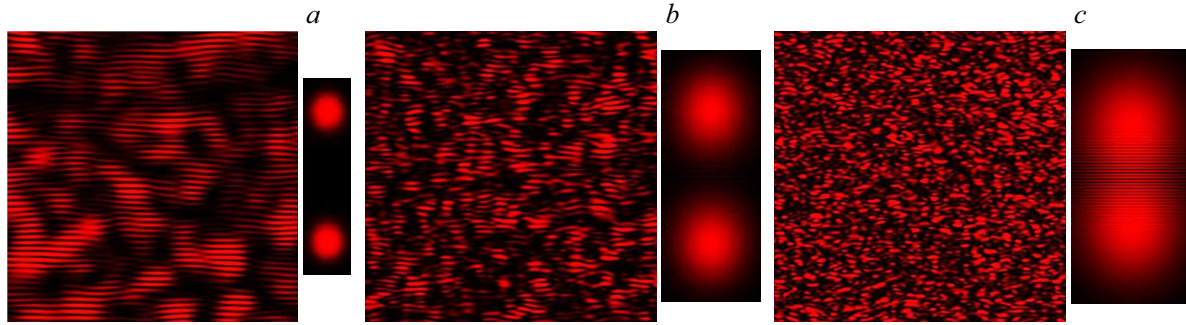


**Figure 2.** Simulated diffraction speckle-modulated interference patterns and images of laser beams in the plane of the scattering surface. The beam waist radius is  $w_0 = 3 \mu\text{m}$ , the distance between centers of illuminating beams on the scattering surface is  $2\Delta y = 40 \mu\text{m}$ . The incidence angles of the beams are  $\pm 30^\circ$ , the wavelength is  $0.63 \mu\text{m}$ . The size of fragments of speckle patterns is  $\sim 3 \times 3 \text{ mm}$ , the distance from the scattering surface to the observation plane is  $100 \text{ mm}$ . Radius  $w$  of the wave surface of illuminating Gaussian beams on the scattering surface is:  $a - 4.5$ ,  $b - 10$ ,  $c - 20 \mu\text{m}$ .

the Gaussian beam and the initial phase  $\varphi_0 = 0$ :

$$\begin{aligned} \varphi_2(x, y, z) = n\pi = & \frac{\pi}{\lambda R_2(y, z)} (x^2 + (y \cos \theta + z \sin \theta)^2) \\ & + \arctg\left(\frac{\lambda(z \cos \theta - y \sin \theta)}{\pi w_0^2}\right) + \frac{2\pi}{\lambda} (z \cos \theta - y \sin \theta), \end{aligned} \quad (4)$$

where

$$R_2(y, z) = (z \cos \theta - y \sin \theta) \left(1 + \left(\frac{\pi w_0^2}{\lambda(z \cos \theta - y \sin \theta)}\right)^2\right).$$

According to formulas (3) and (4), the curves of equal phase in the  $y, x = 0, z$  plane are plotted when Gaussian beams are incident at angles  $\theta = 0^\circ$  and  $\pm 30^\circ$ , which are shown in Fig. 3.

The complex amplitudes  $U_1(x, y, z)$  and  $U_2(x, y, z)$  of the wave fields of the Gaussian beams incident at angles  $\theta$  and  $-\theta$  on the scattering surface of the object and shifted by  $\Delta y$  and  $-\Delta y$ , respectively (Fig. 1), were calculated using the following formulae:

$$\begin{aligned} U_1(x, y, z) = A \frac{w_0}{w_1(y, z)} & \times \exp\left[-\frac{(x^2 + ((y - \Delta y) \cos \theta + z \sin \theta)^2)}{w_1^2(y, z)}\right] \\ & \times \exp\left(i \frac{\pi}{\lambda R_1(y, z)} (x^2 + ((y - \Delta y) \cos \theta + z \sin \theta)^2)\right) \\ & \times \exp\left(i \arctg\left(\frac{\lambda(z \cos \theta - (y - \Delta y) \sin \theta)}{\pi w_0^2}\right)\right) \\ & \times \exp\left(i \frac{2\pi}{\lambda} (z \cos \theta - (y - \Delta y) \sin \theta)\right), \end{aligned} \quad (5)$$

where

$$w_1(y, z) = w_0 \left(1 + \left(\frac{\lambda(z \cos \theta - (y - \Delta y) \sin \theta)}{\pi w_0^2}\right)^2\right)^{0.5},$$

$$R_1 = (z \cos \theta - (y - \Delta y) \sin \theta)$$

$$\times \left(1 + \left(\frac{\pi w_0^2}{\lambda(z \cos \theta - (y - \Delta y) \sin \theta)}\right)^2\right)$$

Taking into account that  $\cos(-\theta) = \cos \theta$  and  $\sin(-\theta) = -\sin \theta$ ,

$$\begin{aligned} U_2(x, y, z) = A \frac{w_0}{w_2(y, z)} & \times \exp\left[-\frac{(x^2 + ((y + \Delta y) \cos \theta - z \sin \theta)^2)}{w_2^2(y, z)}\right] \\ & \times \exp\left(i \frac{\pi}{\lambda R_2(y, z)} (x^2 + ((y + \Delta y) \cos \theta - z \sin \theta)^2)\right) \\ & \times \exp\left(i \arctg\left(\frac{\lambda(z \cos \theta + (y + \Delta y) \sin \theta)}{\pi w_0^2}\right)\right) \\ & \times \exp\left(i \frac{2\pi}{\lambda} (z \cos \theta + (y + \Delta y) \sin \theta)\right), \end{aligned} \quad (6)$$

where

$$w_2(y, z) = w_0 \left(1 + \left(\frac{\lambda(z \cos \theta + (y + \Delta y) \sin \theta)}{\pi w_0^2}\right)^2\right)^{0.5},$$

$$R_2 = (z \cos \theta + (y + \Delta y) \sin \theta)$$

$$\times \left(1 + \left(\frac{\pi w_0^2}{\lambda(z \cos \theta + (y + \Delta y) \sin \theta)}\right)^2\right).$$

To form the random component of the wave field, we specified the complex reflection coefficients of the scattering surface  $\rho_1(x, y) = \rho(x, y - \Delta y)$  and  $\rho_2(x, y) = \rho(x, y + \Delta y)$ , which determine the effect of stochastic amplitude-phase modulation of illuminating laser beams and, accordingly, the effect of scattering of laser beams by a rough surface of an object:

$$\begin{aligned} \rho_1(x, y) &= \rho_{01}(x, y) \exp(iu_1(x, y)), \\ \rho_2(x, y) &= \rho_{02}(x, y) \exp(iu_2(x, y)), \end{aligned} \quad (7)$$

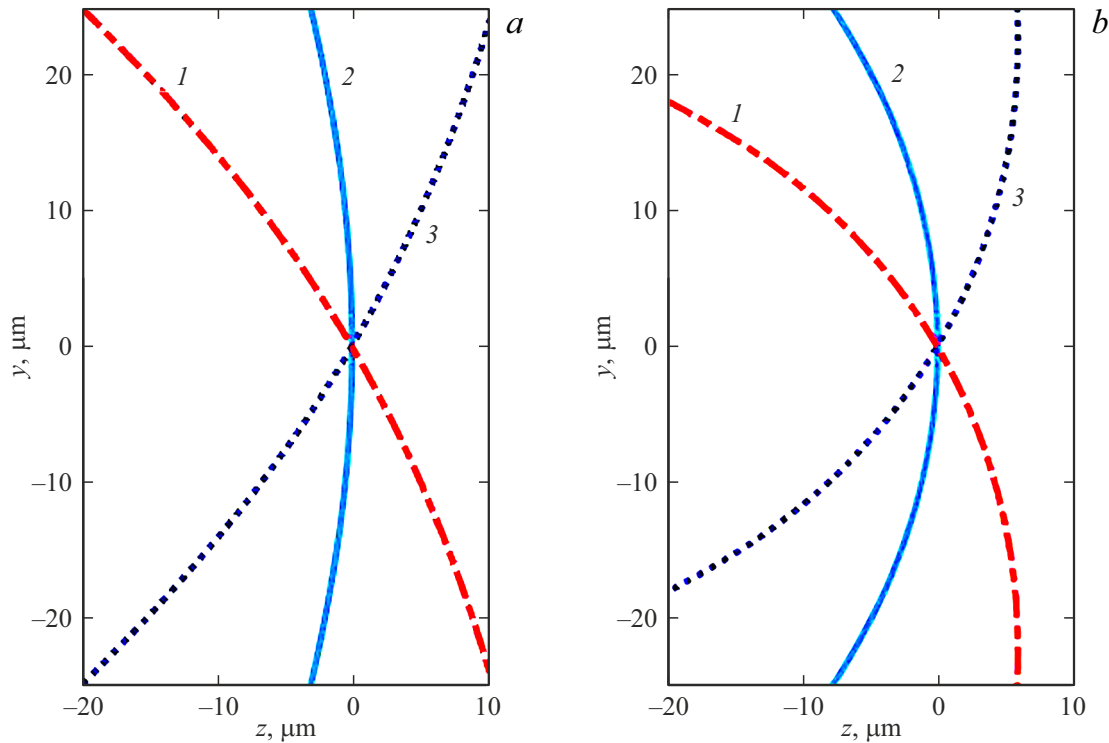


**Figure 3.** Curves of equal phase in the plane  $y, z, x = 0$ , when Gaussian beams are incident at angles  $\theta$ : 1 —  $-30^\circ$ , 2 —  $0^\circ$ , 3 —  $30^\circ$ ,  $n \approx 95$ , beam waist  $w_0$  in  $\mu\text{m}$ : a — 3, b — 2, the distance from the beam waist to the line of equal phase  $30\mu\text{m}$ .

where  $u_1(x, y)$  and  $u_2(x, y)$  are numerical matrices of random independent variables uniformly distributed in the interval from 0 to  $2\pi$ . For simplicity, we can assume that only random phase modulation occurs during reflection from a rough surface, and the amplitude modulation is absent, i.e.  $\rho_0(x, y) \approx 1$ . Thus, the random components of the wave fields arising due to scattering by the surface inhomogeneities were formed as a discrete array of independent circular Gaussian random values [34,35]. The pixel-wise field correlation allows considering such a field actually  $\delta$ -correlated, which most often takes place in real light scattering by rough surfaces with small-scale inhomogeneities.

The wave fields of the Gaussian beams reflected by the scattering surface in the immediate vicinity of the surface (boundary wave fields) can be formally represented as

$$\begin{aligned} U_1(x, y) &= \rho_1(x, y)U_1(x, y), \\ U_2(x, y) &= \rho_2(x, y)U_2(x, y). \end{aligned} \quad (8)$$

In the interference experiment aimed at a local control of surface displacement they often use laser beams focused at the surface or near the surface and the interference signal is detected in the far-field diffraction zone of the scattered wave field. Therefore, to determine the distribution of the total wave field at the interferometer output it is possible to use the Fourier transform of the boundary wave field

formed in the immediate vicinity of the scattering surface:

$$\begin{aligned} U_{1,2}(\xi, \eta) &= \mathbf{F}\{U_{1,2}(x, y)\} = \sum_{x=0}^{M-1} \sum_{y=0}^{N-1} (\rho_1(x, y)U_1(x, y) \\ &+ \rho_2(x, y)U_2(x, y)) \exp \left[ i2\pi \left( x \frac{\xi}{M} + y \frac{\eta}{N} \right) \right], \end{aligned} \quad (9)$$

where  $[M \times N]$  is the dimension of the numerical matrix representing the discrete distribution of complex amplitude in the  $x, y$  plane.

To calculate numerically the complex amplitudes of diffraction fields in the far-field zone of diffraction we used the fast Fourier transform algorithm of the MATLAB system [36]. Construction of full-frame images (Fig. 2), with the aim of visualizing the processes at the output of the speckle interferometer, was carried out using formulas for diffraction transformations for the far-field diffraction zone [37,38]. Simulation of speckle-modulated interference patterns shown in Fig. 2 was performed using Eqs. (1)–(9).

## 2. Modelling the measurement signals of the laser speckle interferometer of transverse displacements of the scattering surface

The spatial intensity distribution of the total diffraction wave field  $I(\xi, \eta)$  at the interferometer output exhibits spatial oscillations, i.e., interference fringes within individual

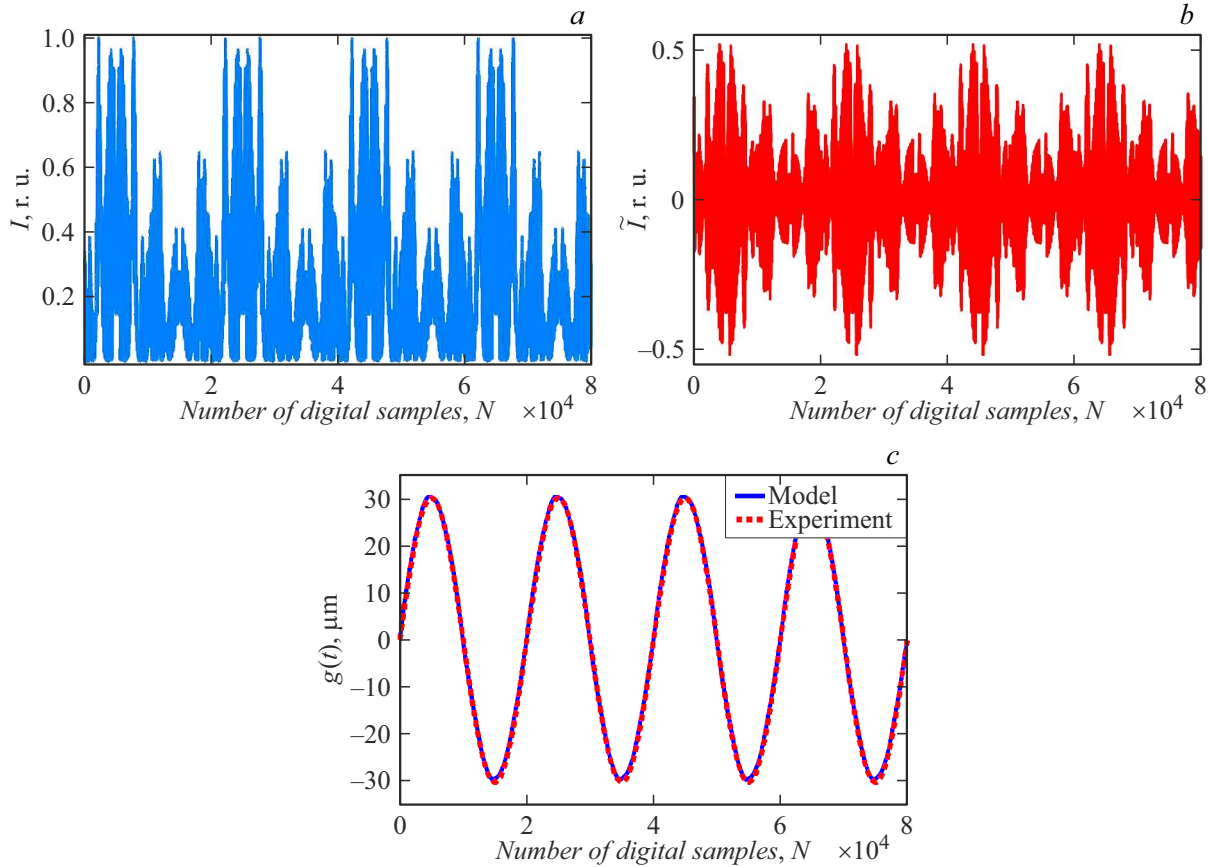


**Figure 4.** Simulated time-dependent interferograms recorded in the far diffraction region when Gaussian illuminating beams with a beam waist radius of  $3\ \mu\text{m}$  are incident on the studied scattering surface subjected to a harmonic displacement (a); the interferogram with subtracted mean value (the variable signal component  $\tilde{I}(N)$ ) (b); plots of the transverse periodic displacement of the scattering surface  $g(t)$ , given and restored from the interferogram  $\tilde{I}(N)$  (c); the laser radiation wavelength is  $\lambda = 0.63\ \mu\text{m}$ .

speckles of the field (Fig. 2). When the transverse displacement  $g$  is time-dependent, the intensity  $I(\xi, \eta, t)$  oscillates at each point of the interference pattern; this oscillation manifests itself in the directed shift of interference fringes in the speckles. Calculating numerically the function  $I(t)$  (temporal oscillogram) at a point with coordinates  $(\xi, \eta)$ , we can extract the displacement  $g(t)$  from the number of oscillations of this function.

Figures 4 and 5 present the temporal numerical interferograms (oscillograms), i.e., intensity curves  $I(t)$ , formed in the region of diffraction at the observation point with coordinates  $\xi = 0$ ,  $\eta = 0$ ,  $z = 100\ \text{mm}$  under periodic transverse displacement  $g(t)$  of the scattering surface with the amplitude  $g_0$ , substantially exceeding the size of laser-illuminated areas on the surface,  $g_0 \gg d$ . High-frequency oscillations of  $I(t)$  in the plots of Fig. 4 cannot be resolved (merge). We can see only low-frequency fluctuations of  $I(t)$ , caused by the change of realizations of the interfering speckle fields at displacements  $g$  exceeding the size  $d$  of areas on the surface illuminated by laser beams,  $g(t) > d$ .

When observing the interference at the output of the interferometer in the near-field diffraction zone rather than in the far-field zone, the complex field amplitude  $U(\xi, \eta, z)$

is determined by the superposition of elementary spherical waves, coming from elementary quasi-point sources — the scattering surface inhomogeneities [37]. According to this concept, it is possible to express the distribution of the total field  $U(\xi, \eta, z)$  at the interferometer output as

$$U(\xi, \eta, z, t) = \sum_{x=0}^{M-1} \sum_{y=0}^{N-1} (\rho_1(x, y, t)U_1(x, y) + \rho_2(x, y, t) \times U_2(x, y)) \frac{\exp[i \frac{2\pi}{\lambda} \sqrt{(x-\xi)^2 + (y-\eta)^2 + z^2}]}{\sqrt{(x-\xi)^2 + (y-\eta)^2 + z^2}}.$$

Interference oscillations of  $I(t)$  at the interferometer output are due to the appearance of different phase shifts  $\varphi_1$  and  $\varphi_2$  in two scattered wave fields upon the displacement of the scattering surface in the direction parallel to the plane of incidence of the laser beams. The wave field formed by a light beam incident on the scattering surface in a direction parallel to the beam incidence plane has a spatial period  $\Lambda_y$  in the surface plane, which depends on the beam incidence angle  $\pm\theta$ ,  $\Lambda_y = \lambda / \sin(\pm\theta)$ . When the scattering surface is displaced by  $g$ , phase shifts  $\varphi = 2\pi(g/\Lambda_y) = 2\pi g \sin(\pm\theta)/\lambda$  appear

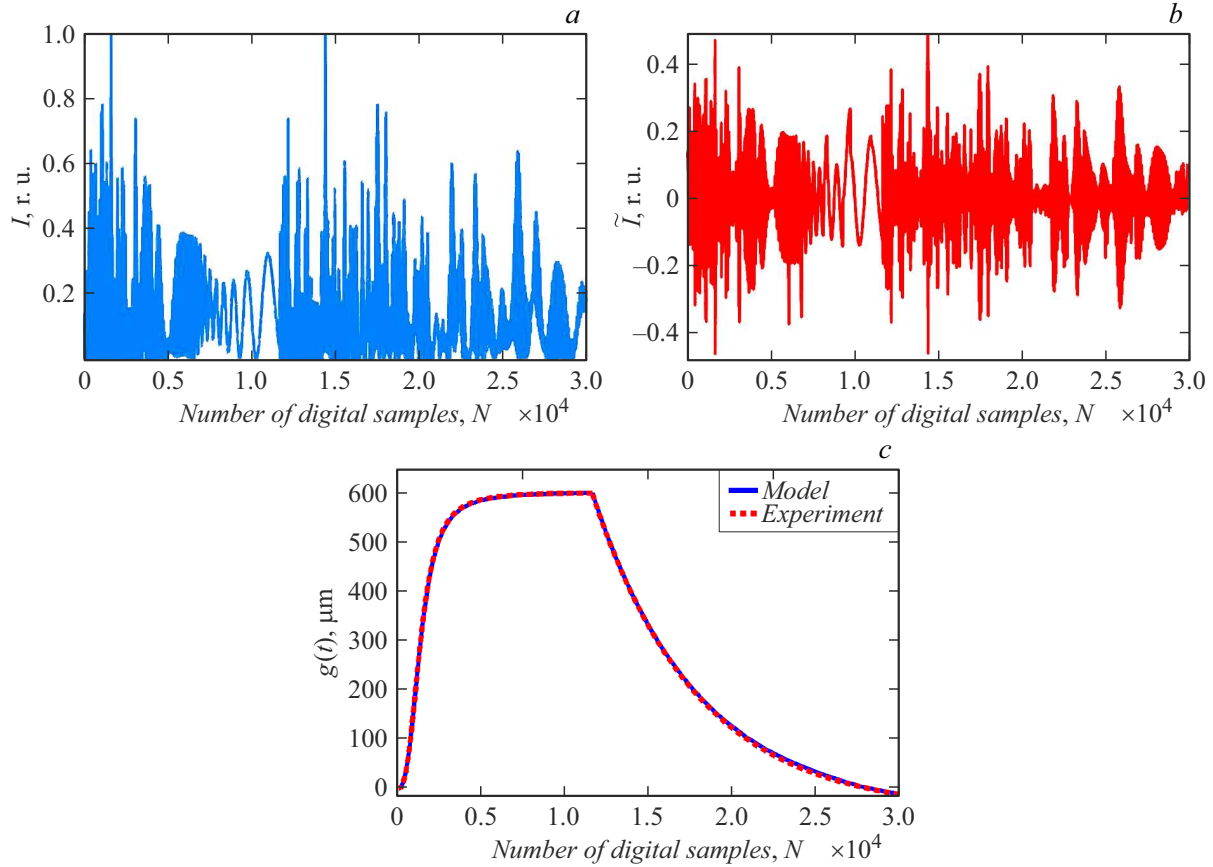


**Figure 5.** Simulated temporal interferograms recorded in the far diffraction region when Gaussian illuminating beams with a beam waist radius of  $3\ \mu\text{m}$  are incident on the studied scattering surface subjected to a harmonic displacement (a); the interferogram with subtracted mean value (the variable signal component  $\tilde{I}(N)$ ) (b); plots of the transverse periodic displacement of the scattering surface  $g(t)$ , given and restored from the interferogram  $\tilde{I}(N)$  (c); the laser radiation wavelength is  $\lambda = 0,63\ \mu\text{m}$ .

in the waves scattered by the surface, so that a phase difference  $\Delta\varphi(g) = \varphi_1 - \varphi_2 = 2\pi g \sin\theta / \lambda$  arises in the wave fields scattered from each laser beam incident on the surface.

The phase difference  $\Delta\varphi(g)$  in the interference experiment is determined by the number of full oscillations or half-oscillations of the field intensity at the interferometer output arising at each change of the phase difference by  $\Delta\varphi(g)$  by  $2\pi$  or by  $\pi$ . Thus, the phase shift  $\Delta\varphi(g) = \pi m$  corresponds to the displacement of the scattering surface by

$$g = m \frac{\lambda}{4 \sin\theta}, \quad (10)$$

where  $m$  is the number of half-oscillations of the time-dependent interferometer signal  $I(t)$  (Fig. 4, a and 5, b).

It is more convenient and precise to count the half-oscillations of the signal  $I(t)$  using the oscillogram  $\tilde{I}(t)$  with subtracted mean values, when the plot passes through zero values (Figs. 4, b and 5, b).

In the numerical experiment, the results of which are shown in Fig. 4, the displacement of the scattering surface  $g(t)$  was set to follow the harmonic law (Fig. 4, c):

$$g(t) = g_0 \sin(2\pi t_N / T), \quad (11)$$

where the amplitude of the object surface displacement was  $g_0 = 30\ \mu\text{m}$ ,  $T$  is the displacement period,  $t_N$  are the moments of time corresponding to counts  $N$ , at which the spatial interferograms (interference patterns) are recorded  $I(\xi, \eta)$ .

To simulate temporal interferograms shown in Fig. 5, the value and the law of the transverse displacement  $g(t)$  of the scattering surface were specified to fit those determined from a natural experiment with heating and subsequent cooling of the object studied [39]. The correctness of the approach used in the numerical simulation is confirmed by the agreement of the simulated and experimental results: the displacement plots in Fig. 5, c obtained from the natural experiment and from simulation coincide with high accuracy.

In the numerical experiment, the values of tangential displacement of the scattering surface  $g_1(t_N) = g_1(N)$  and  $g_2(t_N) = g_2(N)$ , corresponding to the intervals of heating and cooling of the object, were determined using the equations based on the results of the natural experiment:

$$g_1(N) = ab \frac{N^{(1-c)}}{1 + bN^{(1-c)}}, \quad (12)$$

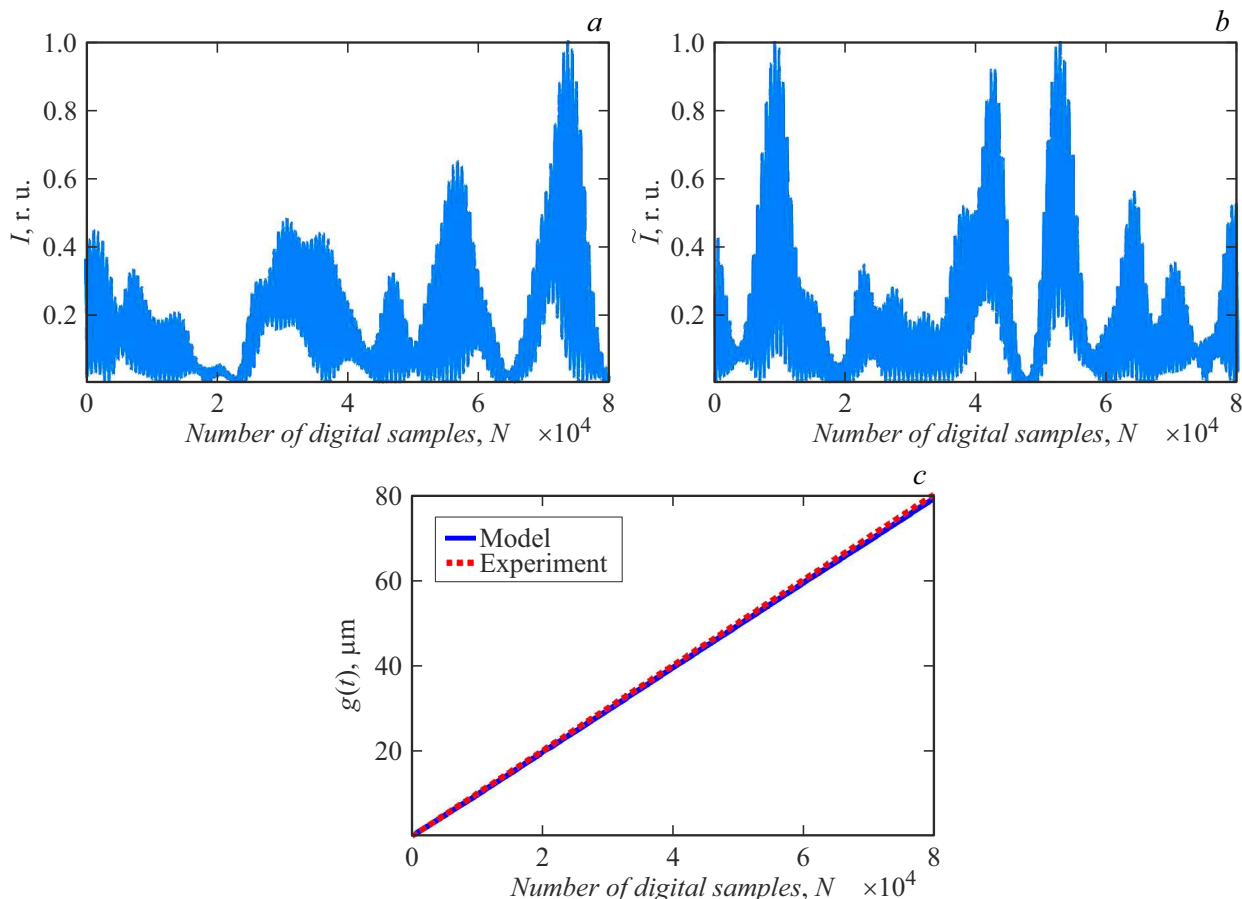


**Figure 6.** Examples of simulated interferograms of uniform transverse displacement of the scattering surface (*a, b*); a plot of a given uniform transverse displacement and a plot of the scattering surface displacement restored from interferograms, averaged over 50 realizations of surface scatterers (*c*). The laser beam waist radius is  $10\ \mu\text{m}$ , the distance between centers of illuminating beams on the scattering surface is  $2\Delta y = 40\ \mu\text{m}$ , the beam incidence angles are  $\pm 30^\circ$ , the wavelength is  $0.63\ \mu\text{m}$ , the distance from the scattering surface to the observation area is  $100\ \text{mm}$ .

$$g_2(N) = a_0 + a_1 \exp\left(-\frac{N - N_2}{t_1}\right) + a_2 \exp\left(-\frac{N - N_2}{t_2}\right) + a_3 \exp\left(-\frac{N - N_2}{t_3}\right), \quad (13)$$

where  $N$  is the number of time count at which a successive interference pattern is recorded. Function  $g_1(N)$  describes a part of the total plot of the scattering surface displacement (Fig. 5, *c*), as a result of its heating from the moment  $N_1 = 0$  of switching the heater on to the moment  $N_2$  of switching the heater off. Function  $g_2(N)$  describes the second, cooling part of the plot, which begins with switching the heater off at  $N_2$ , and lasts till a certain moment  $N_3$ , at which the recording of interference pattern frames is terminated.

The fitting of functions  $g_1(N)$  and  $g_2(N)$  was implemented in the OriginLab environment. An array of natural experiment data on the tangential displacement of the scattering surface of the object was loaded into the program to be used for plotting the displacement magnitude. Then analytical expressions (12) and (13) were chosen for  $g_1(N)$

and  $g_2(N)$ . The functions with the highest determination coefficient of 0.99, which allow reproducing the experimental data with maximum accuracy were used in modeling interference patterns in the numerical experiment. The coefficients in Eqs. (12) and (13) were also chosen in the automated mode. In particular, for numerical modeling of the interferometer signal the following coefficients were obtained and used in Eqs. (12) and (13):  $a = 601.52156$ ;  $b = 7.06915 \cdot 10^{-10}$ ;  $c = -1.90501$ ;  $y_0 = -45.98393$ ;  $a_1 = 1404.79866$ ;  $t_1 = 6195.73625$ ;  $a_2 = 1404.79866$ ;  $t_2 = 6195.73625$ ;  $a_3 = 1404.79866$ ;  $t_3 = 6195.73625$ ;  $N_2 = 11\ 645$ ;  $N_3 = 29\ 849$ .

The results of numerical simulation of the processes of formation of speckle-modulated interference patterns and signals at the output of the speckle interferometer of transverse displacements of a scattering object show good agreement with the results of experimental studies of transverse temperature displacements in the range up to  $600\ \mu\text{m}$ , as evidenced by the coincidence of plots in Fig. 5, *c*.

### 3. Statistical numerical experiment to determine the error in measuring the displacements of a scattering surface

The mathematical model of the interferometer and its signal simulation for known transverse displacements of the scattering surface allow a numerical experiment to estimate the displacement measurement error due to signal fluctuations caused by a change in the realizations of interfering speckle fields, which is practically impossible in a natural experiment. Here, such a statistical numerical experiment was carried out to determine the measurement error for a uniform displacement of the scattering surface. Figure 6 shows interferograms of a uniform transverse displacement of the surface upon various scatterer realizations and the displacement plot averaged over 50 realizations.

In the numerical experiment, a uniform transverse displacement of the scattering surface was specified, the plot of which is shown in Fig. 6, *c*. Then, for a uniform displacement of the scattering surface  $g(t)$  and for the far-field diffraction region, temporal digital interferograms (oscillograms), i. e., the intensity curves  $I(t)$ , were calculated. Having determined the number of half-oscillations from the plot  $I(t)$ , using Eq. (10) we found the displacement of the scattering surface for each moment of time  $t_N$  and obtained the maximum displacement  $g_{\max}$  of the scattering surface. In this way, the random values for subsequent sampling in the statistical experiment were determined. Sampling of random variables was performed at various simulated realizations of the surface scatterers.

The simulation was performed for four different distances from the waists of the light beams to the scattering surface, taken in the range of 45–500  $\mu\text{m}$ . A statistical experiment to estimate the measurement errors for each of the optical scheme parameters was performed with 50 realizations of scatterers, i. e. realizations of speckle fields. The absolute error in measuring the maximum displacement  $\Delta g_{\max}$  was:  $\Delta g_{\max 1} = 3.33 \mu\text{m}$ ,  $\Delta g_{\max 2} = 1.75 \mu\text{m}$ ,  $\Delta g_{\max 3} = -1.4 \mu\text{m}$ ,  $\Delta g_{\max 4} = -0.14 \mu\text{m}$ . The average absolute error in measuring the maximum displacement was  $\Delta g_{\max} = 0.89 \mu\text{m}$ , which determines the relative measurement error  $\approx 0.15\%$ .

In the statistical experiment, two cases of surface illumination are implemented: 1 — illuminated areas on the surface coincide, 2 — illuminated areas on the surface do not overlap. The results for these cases are almost the same.

The largest error in measuring the transverse displacements of the scattering surface is due to fluctuations in the random component of the interferograms, which arise due to the change in the realizations of speckle fields when the surface is displaced by a value exceeding the size  $d$  of the illuminated area on the surface. If, for example, the dimensions of the illumination region are  $d \approx 7 \mu\text{m}$ , then when the scattering surface is displaced by approximately  $7 \mu\text{m}$ , there will be a complete change in the realizations of diffraction speckle fields, which will entail

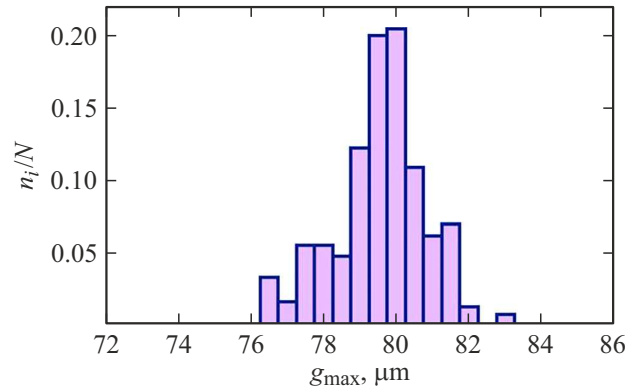


**Figure 7.** Histogram of the distribution of the values of the maximum scattering surface displacement. The sample consists of 900 realizations, the beam waist radius is  $3 \mu\text{m}$ , the distance between centers of illuminating beams on the scattering surface is  $2\Delta y = 20 \mu\text{m}$ , the beam incidence angles are  $\pm 30^\circ$ , the wavelength is  $0.63 \mu\text{m}$ , the maximum specified displacement of the scattering surface is  $80 \mu\text{m}$ , the distance from the scattering surface to the observation area is 100 mm.

a random change in amplitudes and phases of interfering waves. The field phase difference will change with equal probability by a random value in the interval  $[-\pi, \pi]$ . Consequently, there will be a random change in both the amplitude of the oscillations, and their shift on the interferogram — not by a jump, but smoothly, as can be seen from the amplitude of the oscillations in Fig. 6, *a, b*. If the total displacement is  $80 \mu\text{m}$ , then there will be approximately  $80/7 \approx 11$  of such random oscillation displacements. According to Eq. (11), each displacement gives an error  $\approx \lambda/2 \sin \theta = 0.63 \mu\text{m}$  in the shift of the scattering surface. From here we obtain a rough estimate of the expected total maximum error  $0.63 \cdot 11 \approx 6.9 \mu\text{m}$ .

For a more accurate estimate of the measurement error resulting from a change in the realizations of speckle fields, a sample of  $m = 900$  oscillograms of uniform transverse displacement of the surface was formed with different realizations of surface scatterers. Figure 7 shows a histogram of the distribution of the scattering surface maximum displacements, based on a sample of 900 values.

In modeling based on  $m = 900$  scatterer realizations, the mean arithmetic value of the maximum displacement determined from the oscillograms is  $\langle g \rangle \approx 79.56 \mu\text{m}$ . The deviation of the average value of the maximum displacement from that specified in the simulation is  $\Delta g \approx 0.44 \mu\text{m}$ . The best estimate of the average measurement deviation is the average measurement error  $\langle \Delta g \rangle$  [40].

$$\langle \Delta g \rangle = \frac{1}{m} \sum_{i=1}^m |g_i - \langle g \rangle|. \quad (15)$$

In the numerical experiment performed with a sample of  $m = 900$ , the average measurement deviation was  $\langle \Delta g \rangle \approx 1.0 \mu\text{m}$ , which corresponds to an average relative

measurement error of  $\approx 1.26\%$ . The small relative measurement error obtained in the experiment confirms the validity of the approach used in modeling processes in the interferometer of transverse displacement of the scattering surface.

## Conclusion

We report computer simulation of a speckle interferometer for measuring transverse microdisplacements of the scattering object surface. Computer simulation is implemented based on diffraction transformations of wave fields in an optical interference system implying digital recording of speckle-modulated spatiotemporal interference pattern signals. Oscillograms of the transverse displacement of the scattering surface are obtained for various laws of motion, which are formed in the far-field diffraction region when Gaussian laser beams are incident on the scattering surface under study.

Numerical simulation of the speckle-modulated interference patterns and signals at the output of a speckle interferometer of transverse displacement of a scattering object illuminated by Gaussian laser beams allows revealing the properties and quantitative parameters of the interference measurement signals. The simulation results agree with those of natural experiment, in which transverse surface displacements of up to  $600\ \mu\text{m}$  were induced by heating and cooling the sample.

The mathematical model developed here makes allows estimating the measurement errors associated with fluctuations in the random component of time-dependent interferograms caused by the change of realizations of the interfering speckle fields. The processes of mutual decorrelation of speckle-modulated diffraction wave fields, which form the interference signal at the output of the speckle interferometer during the object motion, are modeled, and the influence of these processes on the occurrence of the maximum possible measurement error is analyzed. The statistical numerical experiment performed made it possible to quantify the average measurement error of the transverse displacement speckle interferometry method, which arises due to the decorrelation of wave fields at the output of the interferometer.

The mathematical model of the speckle interferometer of transverse microdisplacements, based on diffraction transformations of wave fields, shows that the measuring signal at the output of the interferometer arises as a result of a deterministic change in the phases of interfering wave fields, which makes it possible not to use the concepts of the Doppler effect to explain the principle of the interferometer operation.

Numerical experiments on modeling the transverse-displacement speckle interferometer are an effective tool for developing optical interference methods for non-contact analysis, measurement and control of microdeformations and microdisplacements of objects.

## Funding

The work was carried out within the framework of the State Assignment of the Ministry of Science and Higher Education of the Russian Federation (theme „Precision diagnostics, sensors and process control in technical and living systems based on photonic technologies, including the solution of thermophysical problems“, № 121022000123-8).

## Conflict of interest

The authors declare that they have no conflict of interest.

## References

- [1] J.W. Goodman. *Speckle Phenomena in Optics: Theory and Applications* (SPIE PRESS, Washington, 2020)
- [2] M. Françon. *La Granularite Laser (Spekle) et Ses Applications en Optique* (Masson, Paris, 1978)
- [3] H.J. Rabal, R.A. Braga (ed.). *Dynamic Laser Speckle and Applications* (CRC Press, Taylor and Francis Group, NY., 2009)
- [4] W. Osten (ed.). *Optical Inspection of Microsystems* (CRC Press, Taylor and Francis Group, NY., 2007)
- [5] P. Jacquot. *Strain*, **44** (1), 57 (2008). DOI: 10.1111/j.1475-1305.2008.00372.x
- [6] R. Jones, C. Wykes. *Holographic and Speckle Interferometry* (Cambridge University Press, 1989)
- [7] Razumovskii I.A. *Interferentsionno-opticheskiye metody mekhaniki deformiruyemogo tverdogo tela* (Izd-vo MGTU, M., 2007) (in Russian).
- [8] Klimentko I.S. *Golografiya sfokusirovannykh izobrazheniy i spekl-interferometriya* (Nauka, M., 1985) (in Russian).
- [9] A. Donges, R. Noll. *Laser Measurement Technology* (Springer, Berlin, 2015), v. 188.
- [10] C. Joenathan, R.S. Sirohi, A. Bernal. *The Optics Encyclopedia. Advances in Speckle Metrology* (Wiley, New Jersey, 2015). DOI: 10.1002/9783527600441.oe087.pub2
- [11] A.P. Vladimirov. *Opt. Eng.*, **55** (12), 121727 (2016). DOI: 10.1117/1.oe.55.12.121727
- [12] Kulchin Yu.N. Vitrik O.B., Kamshilin A.A., Romashko R.V. *Adaptivnyye metody obrabotki spekl-modulirovannykh opticheskikh poley* (Fizmatlit, M., 2009) (in Russian).
- [13] A. Boutier. *Laser Velocimetry in Fluid Mechanics* (Wiley, London, 2013)
- [14] A.P. Vladimirov, V.I. Mikushin, A.L. Lisin. *Tech. Phys. Lett.*, **25** (12), 1008 (1999). DOI: 10.1134/1.1262710
- [15] J. Stempin, A. Tausendfreund, D. Stöbener, A. Fischer. *Nanomanuf. Metrol.*, **4**, 237 (2021). DOI: 10.1007/s41871-020-00093-0
- [16] Y. Arai. *Opt. Eng.*, **54** (2), 024102 (2015). DOI: 10.1117/1.OE.54.2.024102
- [17] K. Zhu, B. Guo, Y. Lu, S. Zhang, Y. Tan. *Optica*, **4** (7), 729 (2017). DOI: 10.1364/OPTICA.4.000729
- [18] L.P. Tendela, G.E. Galizzi. *Opt. Lasers Eng.*, **110**, 149 (2018). DOI: 10.1016/j.optlaseng.2018.05.023
- [19] H.-L. Hsieh, P.-C. Kuo. *Opt. Exp.*, **28** (1), 724 (2020). DOI: 10.1364/OE.382494
- [20] P. de Groot, X. Colonna de Lega, J. Kramer, M. Turzhitsky. *Appl. Opt.*, **43** (25), 4821 (2004). DOI: 10.1364/AO.43.004821

- [21] T. Pahl, S. Hagemeyer, M. Künne, D. Yang, P. Lehmann. *Opt. Exp.*, **28** (28), 39807 (2020). DOI: 10.1364/OE.411167
- [22] P.J. de Groot, X. Colonna de Lega. *J. Opt. Soc. Am. A*, **37** (9), B1 (2020). DOI: 10.1364/JOSAA.390746
- [23] D.V. Lyakin, L.A. Maksimova, V.P. Ryabukho. *Opt. Spectr.*, **127**, 571 (2019). DOI: 10.1134/S0030400X19090170
- [24] G.N. Vishnyakov, A.D. Ivanov, G.G. Levin, V.L. Minaev. *Quant. Electr.*, **50** (7), 636 (2020). DOI: 10.1070/QEL17281
- [25] Grizbil B.A., Maksimova L.A., Ryabukho V.P. *Komp. opt.*, **44** (4), 568 (2020) (in Russian). DOI: 10.18287/2412-6179-CO-702.
- [26] D.J. Burrell, M.F. Spencer, N.R. Van Zandt, R.G. Driggers. *Appl. Opt.*, **60** (25), G64 (2021). DOI: 10.1364/AO.427963
- [27] Dubnishchev Yu.N., Rinkevichius B.S. *Metody lazernoy doplerovskoy anemometrii* (Nauka, M., 1982) (in Russian).
- [28] Rinkevichius B.S. *Lazernaya diagnostika potokov* (Izd-vo MEI, M., 1990) (in Russian).
- [29] Dubnishchev Yu.N. *Lazernyye doplerovskiye izmeritel'nyye tekhnologii* (NGTU, Novosibirsk, 2002) (in Russian).
- [30] Y.N. Dubnishchev, T.Y. Dubnishcheva, V.G. Nechaev. *Optoelectronics, Instrumentation and Data Processing*, **56** (4), 333 (2020). DOI: 10.3103/S8756699020040056
- [31] A. Boutier. *Laser Velocimetry in Fluid Mechanics* (Wiley, London, 2013)
- [32] Meledin V.G. *Interesko Geo-Sibir*, **2** (5), 141 (2018) (in Russian).
- [33] Korolenko P.V. *Optika kogerentnogo izlucheniya* (Izd-vo MGU, M., 1997) (in Russian).
- [34] O. Korotkova. *Random Light Beams: Theory and Applications* (Boca Raton, FL: CRC Press, 2014)
- [35] J.W. Goodman. *Statistical Optics* (Wiley, NY., 2000)
- [36] E.C. Ifeachor, B.W. Jarvis. *Digital Signal Processing. A Practical Approach*. 2nd ed. (Prentice Hall, Pearson Education Limited, 2002)
- [37] M. Born, E. Wolf. *Principles of Optics. Electromagnetic Theory of Propagation, Interference and Diffraction of Light*. 7th ed. (Cambridge University Press, 1999)
- [38] J.W. Goodman. *Introduction to Fourier Optics*. 3 ed. (Roberts and Company Publishers, 2005)
- [39] Zhuravlev S.D., Bogachev R.Yu., Rogovin V.I., Petrosyan A.I., Shesterkin V.I., Grizbil B.A., Ryabukho V.P., Zakharov A.A.. *Elektronika i mikroelektronika SVCh*, **1**, 170 (2018) (in Russian).
- [40] Novitsky P.V., Zograph I.A. *Otsenka pogreshnostey rezultatov izmereniy* (Energoatomizdat, L., 1991) (In Russian)

*Translated by Ego Translating*